Photosynthesis Research **48**: 367–377, 1996.

Regular paper

Tubular exciton models for BChl *c* antennae in chlorosomes from green photosynthetic bacteria

Daniel R. Buck & Walter S. Struve
Ames Laboratory-USDOE and Department of Chemistry, Iowa State University, Ames, IA 50011, USA

Received 7 November 1995; accepted in revised form 4 March 1996

Key words: aggregates, bacteriochlorophyll *c*, *Chloroflexus aurantiacus*, chlorosomes, green photosynthetic bacteria

Abstract

Exciton calculations on tubular pigment aggregates similar to recently proposed models for BChl *c/d/e* antennae in light-harvesting chlorosomes from green photosynthetic bacteria yield electronic absorption spectra that are superimpositions of linear J-aggregate spectra. While the electronic spectroscopy of such antennae differs considerably from that of linear J-aggregates, tubular exciton models (which may be viewed as cross-coupled J-aggregates) may be constructed to yield spectra that resemble that of the BChl *c* antenna in the green bacterium *Chloroflexus aurantiacus*. Highly symmetric tubular models yield absorption spectra with dipole strength distributions essentially identical to that of a J-aggregate; strong symmetry-breaking is needed to simulate the absorption spectrum of the BChl *c* antenna.

Abbreviations: BChl – bacteriochlorophyll; [E,M] BChl c_S – bacteriochlorophyll *c* with ethyl and methyl substituents in the 8- and 12-positions, and with stearol as the esterifying alcohol

Introduction

The bacteriochlorophyll (BChl) *c*, *d*, and/or *e* antennae in light-harvesting chlorosomes of green photosynthetic bacteria are unique, in that proteins appear to be little involved in their pigment organization. Such antennae appear to be BChl oligomers, in which the pigments are directly bound together by coordination of the Mg atom on one pigment to hydroxyl and/or keto groups on adjacent pigments (Bystrova et al. 1979; Smith et al. 1983; Blankenship et al. 1988; Lutz and van Brakel, 1988; Brune et al. 1988). While numerous models have been proposed for the local pigment binding modes, many of the earlier models have been ruled out because the Mg atom is now known to be pentacoordinate, and because the 13^1 keto group and the 3^1 OH group have been shown to be directly involved in the aggregation (Blankenship et al. 1995). Of the two models that are consistent with FTIR and resonance Raman spectra of BChl aggregates (Brune et al. 1988), one visualizes the BChl pigments as being arranged in dual antiparallel chains. Molecules within each chain are linked by H-bonds between 13^1 keto and 3^1 OH groups, and the antiparallel chains are crosslinked by ligation of Mg atoms with hydroxyl groups. The second model, which also involves dual chains, invokes similar H-bonding between pigments in the same chain and similar crosslinking. However, the pigment orientations in the two chains are nearly parallel, rather than antiparallel.

Several groups (Nozawa et al. 1993; Matsuura et al. 1993; Nozawa et al. 1994; Hozwarth and Schaffner 1994) have proposed large-scale models for organization of the pigments into supramolecular structures of size commensurate with that of BChl rodlike elements that are visible under electron microscopy (Staehelin et al. 1978). In some cases, the macrocycle planes are envisaged to be perpendicular to the cylindrical rod surface; in others, they are tangent to the surface. The models also differ in the orientations of the ester-

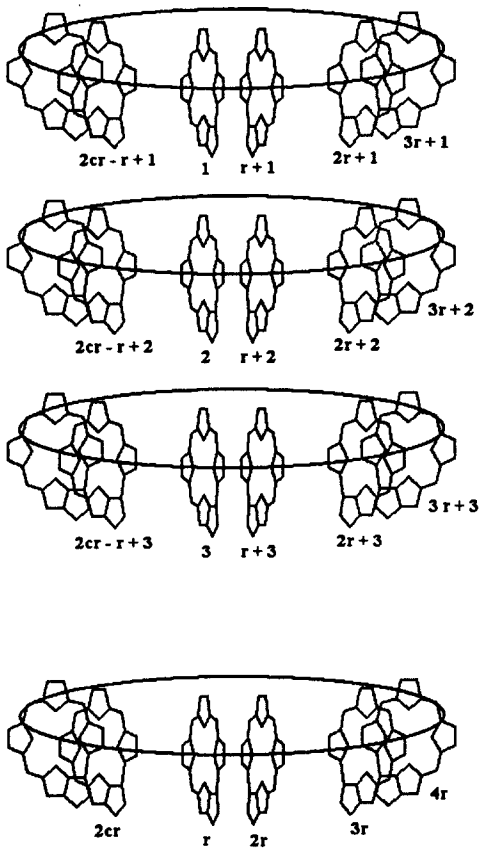

Figure 1. Pigment numbering scheme for tubular aggregate with pigments arranged in $2c$ columns containing r pigments each. For the models described in Figures 4–6 below, the Hamiltonian matrix elements are $H_{i,i+r} = b_1$ for $1 < i < r$, $(2r + 1) < i < 3r$, $(4r + 1) < i < 5r$, ... ; $H_{i,i+r} = b_2$ for $(r + 1) < i < 2r$, $(3r + 1) < i < 4r$, ... , $(2c - 1)r + 1 < i < 2cr$; and $H_{ij} = a$ for adjacent pigments in the same column. All other off-diagonal matrix elements are zero. For definiteness, the macrocycle planes are drawn normal to the cylinder surface; the theory is also applicable to aggregates in which the planes are tangent to the surface. Transition moment orientations are those for case (a), cf. Figure 2 and text.

ifying alcohol chains; these are variously described as occupying the center of the cylinder, radiating outward from the cylinder surface, and alternating between the inward and outward directions. A common feature of these models is the arrangement of BChl Q_y transition moments essentially parallel or antiparallel to the rod axis. This is consistent with linear dichroism studies of oriented chlorosomes from the green bacterium *Chloroflexus aurantiacus*, which show that the BChl *c* Q_y transition moments make an average angle of 17° with respect to the chlorosome long axis (van Amerongen et al. 1988). Similarly, the initial anisotropy $r(0)$ in pump-probe studies of the BChl *c* antenna in chlorosomes from *Cf. aurantiacus* is very close to 0.4, which is the predicted value for a strongly coupled antenna composed of collinear pigments (Savikhin et al. 1994). The anisotropy for BChl *c* absorption wavelengths typically exhibits minimal subsequent decay ($r(\infty) \sim 0.37$), indicating the presence of significant long-range ordering as well.

The oligomeric light-harvesting antennae in chlorosomes from *Cf. aurantiacus* appear to be simpler in several respects than those in other green photosynthetic bacteria, and thus may be a prototype for understanding the large-scale antenna structure. Their pigment composition is relatively uniform (predominantly [E,M] BChl c_S, with small amounts of BChl *c* pigments having geranylgeraniol and phytol instead of stearol as the esterifying group). They exhibit considerably more long-range BChl pigment order than oligomeric antennae from green sulfur bacteria (van Noort et al. 1994; Savikhin et al. 1995). The extent of inhomogeneous broadening in the BChl *c* antenna of chlorosomes from *Cf. aurantiacus* remains unsettled. Spectral hole-burning and pump-probe studies suggest that the BChl *c* absorption spectrum is dominated by homogeneous rather than inhomogeneous broadening in *Cf. aurantiacus* (Fetisova and Mauring, 1992; Savikhin et al, 1994). However, since the BChl *c* Q_y linear dichroism of oriented chlorosomes from *Cf. aurantiacus* varies somewhat with wavelength, Matsuura et al. (1993) proposed that energy transfer occurs among several well-defined BChl *c* spectral forms. Spectral heterogeneity appears to be strongly asserted in the oligomeric antennae of green sulfur bacteria (van Noort et al. 1994; Savikhin et al. 1995a).

While the BChl *c* linear dichroism of chlorosomes from *Cf. aurantiacus* suggests that the transition moment organization resembles that of a linear J-aggregate chain (van Amerongen et al. 1988), the BChl *c* electronic spectrum of intact chlorosomes shares little in common with the J-aggregate spectrum. The oscillator strengths for transitions from the ground state to the one-exciton levels of a large, linear J-aggregate are heavily concentrated in the lowest-energy level (Mimuro et al. 1989; Lin et al. 1991; Alden et al. 1992; Somsen 1995). By contrast, the lowest exciton component in spectral hole-burning of the BChl *c* antenna of whole cells from *Cf. aurantiacus* occurs near 752 nm, in a spectral region of relatively low absorption strength. The band maximum in the absorption spectrum (which exhibits $\sim$90 cm^{-1} inhomogeneous broadening at most) occurs near 742 nm. Hence, the BChl *c* antenna must exhibit more than one exciton component with substantial oscillator strength, and

the most intense electronic transition must occur at an energy significantly higher (by ~170 cm^{-1}) than that of the lowest-energy exciton component. While there is still disagreement about the extent of spectral heterogeneity in the BChl *c* oligomers in *Cf. aurantiacus* (Fetisova and Mauring 1992; Matsuura et al. 1993), we consider here whether a tubular exciton model for a spectrally homogeneous BChl *c* antenna can account for its steady-state Q_y absorption spectrum.

The exciton model

The position of each pigment in our cylindrical aggregate model can be described by a single index *i*, as shown in Figure 1. The tubular aggregate is visualized as a stack of *r* disks, each containing 2*c* pigments distributed on the periphery of a ring. The aggregate contains 2*cr* pigments. Pigments 1 through *r* occupy an axial line (or column) on the cylinder surface; pigments (*r* + 1) through 2*r* occupy a parallel, neighboring column; and so on up to pigments [(2*c* − 1)*r* + 1] through 2*cr*, which occupy a column adjacent to the one that contains pigments 1 through *r*. The resonance couplings between pigments depend on the Q_y transition moment directions μ_i, μ_j and on their separation *R* via

$$H_{ij} = \frac{\mu_i \cdot \mu_j - 3(\mu_i \cdot \hat{R})(\mu_j \cdot \hat{R})}{R^3} \qquad (1)$$

in the point dipole-dipole approximation.

In our simplest model, the couplings are assumed to be non-zero only for nearest-neighbor pigments. (The effects of including non-nearest neignbor interactions are considered below.) The diagonal energies H_{ii} are assumed to be uniform for all pigments. The off-diagonal elements H_{ij} are set equal to *a* for adjacent pigments on the same axial line on the cylinder surface, and equal to zero for all other pairs *(i,j)* on the same line. H_{ij} is modeled as b_1 for pairs of pigments *(i,j)* belonging to the same disk, positioned on the first and second axial lines, on the third and fourth, on the fifth and sixth, etc. H_{ij} is set equal to b_2 for pairs of pigments *(i,j)* belonging to the same disk, positioned on the second and third axial lines, on the fourth and fifth lines, etc. up to the 2*c*th and first lines. The pigments are thus grouped into pairs of linear aggregates, with uniform intra-aggregate interactions *a* and alternating inter-aggregate interactions b_1 and b_2. For $b_1 \neq b_2$, our model therefore considers dual chains similar to the ones proposed by Brune et al. (1988). In the case where $a < 0$ and $b_1 = b_2 = 0$, one recovers a set of 2*c* non-interacting J-aggregates; the case $a > 0$ and $b_1 = b_2 = 0$ would describe a set of 2*c* non-interacting H-aggregates. The signs of *a*, b_1, and b_2 depend on the pigment orientations (Equation (1)). We consider the three cases shown in Figure 2 for the pigment orientations: (a) one in which all of the transition moments are collinear with the rod symmetry axis – i.e. $a < 0$ and b_1, $b_2 > 0$; (b) one in which all of the transition moments are either parallel or antiparallel to the symmetry axis, and pigments occupying adjacent lines are mutually antiparallel – i.e. *a*, b_1, $b_2 < 0$; and (c) one in which pigments belonging to the same pair of linear aggregates are antiparallel, whereas adjacent pigments belonging to neighboring pairs of linear aggregates are parallel – i.e. *a* , $b_1 < 0$, and $b_2 > 0$. (The latter case is topologically possible only for an even number *c* of pigment pairs per disk, i.e. 2*c* = 4, 8, 12, ...) We emphasize at the outset that these cases (in which the Hamiltonian belongs to either the $\mathbf{D}_{2c,h}$ or $\mathbf{D}_{ch}$ point group, depending on b_1 and b_2) are only the most symmetric ones possible for a tubular aggregate. Additional symmetry-breaking proves to be necessary for simulation of realistic absorption spectra (see below).

In the special case of a cylinder containing 2*c* uncoupled J-aggregates of length *r* ($a < 0$, $b_1 = b_2 = 0$), the *r* energy eigenvalues for the one-exciton components are known to be (Lin et al. 1991)

$$E_i = E_0 \pm 2a\cos\left(\frac{\pi}{r+1}\right),$$
$$E_0 \pm 2a\cos\left(\frac{2\pi}{r+1}\right),$$
$$E_0 \pm 2a\cos\left(\frac{3\pi}{r+1}\right),$$
$$\ldots, (E_0) \qquad (2)$$

here the eigenvalue E_0 (the unperturbed Q_y transition energy) exists if *r* is odd. The one-exciton states in a linear J-aggregate of length *r* may be expanded in terms of the single-pigment excitations Φ_j as

$$\Psi_i = \sum_{j=1}^{r} c_{ij}\Phi_j \qquad (3)$$

where the expansion coefficients are (Lin et al. 1991)

$$c_{ij} = \left(\frac{2}{r+1}\right)^{1/2} \sin\left(\frac{ij\pi}{r+1}\right) \qquad (4)$$

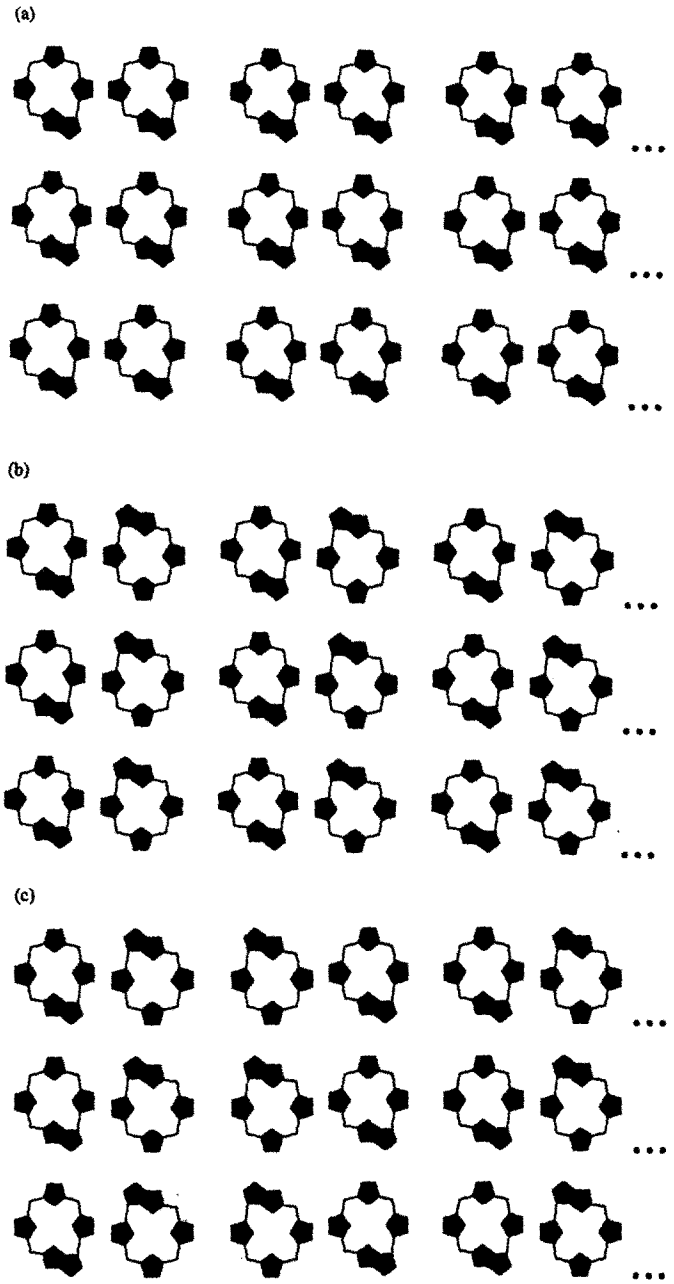

Figure 2. Transition moment directions for cases (a) through (c) considered in text. The tubular aggregate axis is vertical, and all BChl *c* Q_y transition moments are either parallel or antiparallel to this axis. This figure is only intended to show relative transition moment directions; the BChl *c* macrocycle planes may be rotated at any angle about their transition moments.

In this context, exciton components $i = 1$ and r correspond to the lowest- and highest-energy exciton levels in a linear J-aggregate, where the resonance coupling $a < 0$.[1] The reverse is true in an linear H-aggregate ($a > 0$). The J-aggregate exciton levels become more widely spaced as i increases from 1 to $\sim r/2$, producing a convergent band series (Equation (2) and Figure 3). It may be shown (Lin et al. 1991) that for a J-aggregate in the limit of large r, the transition from the ground state to the lowest one-exciton level contains a fraction $8/\pi^2 = 0.81$ of the sum of dipole strengths for transitions from the ground state to all one-exciton levels. In the same limit, the transition from the ground state to exciton component i has the fractional dipole

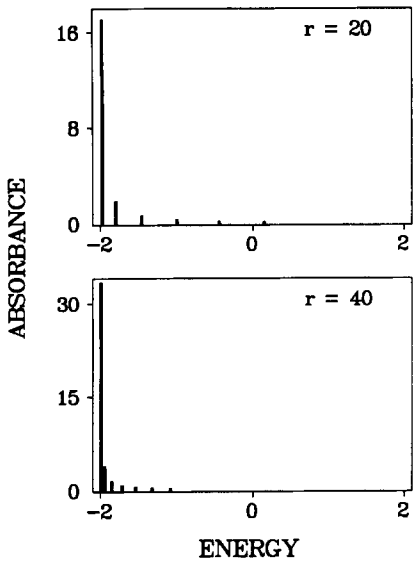

Figure 3. Schematic absorption spectra for linear J-aggregate, with $a < 0$ and $r = 20$ (top) and $r = 40$ (bottom). Energy scale is in units of $|a|$, and diagonal energies are zero. The satellite bands coalesce with the bandhead in the limit of large r. For simplicity, only the first few satellite bands (corresponding to $i = 3, 5, 7, ...$) are shown for each bandhead ($i = 1$) in Figures 3–9. The band intensities sum to the number of pigments (20 and 40 in the top and bottom panels, respectively).

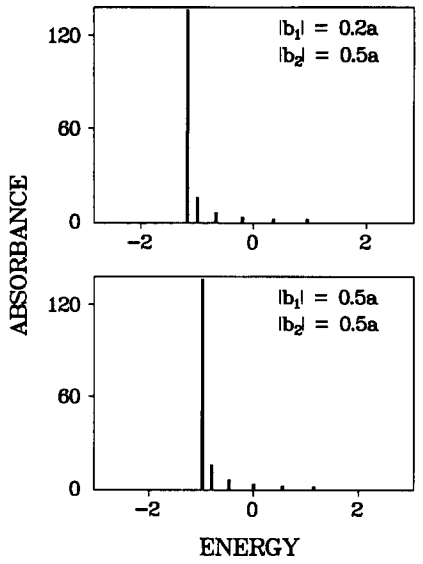

Figure 4. Schematic absorption spectra for a 160-pigment tubular aggregate containing $r = 20$ disks with $2c = 8$ pigments each. Couplings are (from top) $|b_1| = -0.2a$, $|b_2| = -0.6a$; and $|b_1| = |b_2| = -0.5a$. Energy scale is in units of $|a|$; energies are relative to the diagonal energies, which are taken to be zero. The lowest-energy exciton components (not discernible in this Figure) occur at energies (from top) $-2.74|a|$ and $-2.98|a|$. The band intensities sum to 160, the number of pigments.

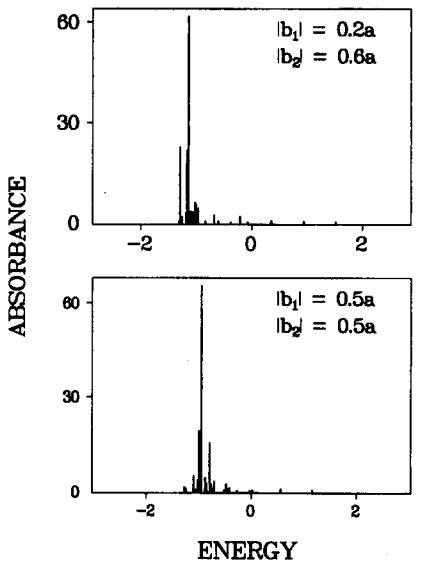

Figure 5. Schematic absorption spectra for the same tubular aggregates as in Fig. 4, except that random components with range $\pm 0.4|b_1|$ and $\pm 0.4|b_2|$ have been added to the couplings b_1 and b_2.

strength $8/i^2\pi^2$ for odd i, and 0 for even i. As shown in Figure 3, this produces a J-aggregate spectrum in which most of the dipole strength is concentrated in the lowest exciton component. (For H-aggregates, the highest-energy exciton level carries most of the oscillator strength instead.) In the limit of infinite r, the higher-energy optically allowed exciton components in a J-aggregate coalesce into the lowest-energy component, with the result that only a single optically allowed transition occurs (Somsen 1995). For future reference, we will use the term *bandhead* to denote the most intense ($i = 1$) J-aggregate band; the higher-energy bands ($i > 1$) will be termed *satellite bands*. In view of Equation (1), the lowest-energy exciton component is red-shifted by essentially $2a$ from E_0 in a linear J-aggregate when r is large. The J-aggregate model itself is clearly unsatisfactory if the BChl *c* antenna spectrum is homogeneously broadened, because it does not explain why the lowest-energy exciton component lies $\sim 170\ \text{cm}^{-1}$ below the BChl *c* Q_y absorption band maximum in whole cells from *Cf. aurantiacus* (Fetisova and Mauring 1992).

When non-zero couplings b_1, b_2 are introduced among the $2c$ linear aggregates, the single J-aggregate band series is split into $2c$ series. The energy spacings of bands within each series are still given by Equation (2) in terms of a and the aggregate length r. The distribution of band intensities within each series also remains the same as that in a linear J-aggregate.

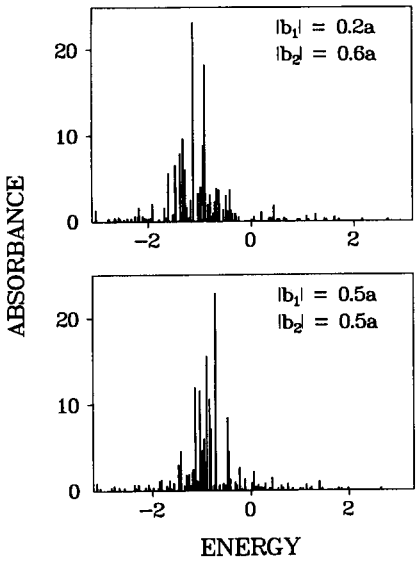

Figure 6. Schematic absorption spectra for the same tubular aggregates as in Fig. 4, except that diagonal energies H_{ii} are random numbers between $-|a|$ and $+|a|$.

The bandhead positions (relative to that of the unshifted bandhead for $b_1 = b_2 = 0$) are given by $b_1 + b_2$, $b_1 - b_2$, $-b_1 + b_2$, $-b_1 - b_2$, $\pm\sqrt{b_1^2 + b_2^2}$ when $2c = 8$, and by $b_1 + b_2$, $b_1 - b_2$, $-b_1 + b_2$, $-b_1 - b_2$, $\pm\sqrt{b_1^2 + b_1 b_2 + b_2^2}$, $\pm\sqrt{b_1^2 - b_1 b_2 + b_2^2}$ when $2c = 12$. (Each of the irrational eigenvalues is doubly degenerate.) However, only the bandhead at $|b_1| + |b_2|$ is dipole-allowed; the other $2c-1$ bandheads (and their satellite bands) are symmetry-forbidden. For these highly symmetric aggregates, the presence of non-zero interactions b_1, b_2 still yields only one allowed J-aggregate series. Figure 4 shows simulated absorption spectra for aggregates of 160 pigments, arranged in 20 disks containing 8 pigments each. In case (a) – where all of the pigment transition moments are collinear and b_1, b_2 are both positive – the allowed bandhead transition lies $2(b_1 + b_2)$ to the blue of the lowest exciton component, which is situated at $-(b_1 + b_2)$ relative to the unsplit J-aggregate bandhead (Figure 4). The horizontal energy scales in Figures 3–4 were chosen to bracket the entire range of eigenvalues, irrespective of oscillator strength. Hence, the presence in Figure 4 of spectral regions at the low-energy end without discernible oscillator strength indicates the presence of low-lying, optically forbidden transitions. In this model, increasing the interactions b_1,b_2 relative to $|a|$ shifts the transitions with appreciable oscillator strengths toward the blue edge of the spectrum. In case (b) – where all of a, b_1, and b_2 are negative – and in case (c) – where $b_1 < 0$ and $b_2 > 0$ – the allowed bandhead is still located at $|b_1| + |b_2|$. The spectra in these cases are thus identical to that in case (a) for given $|b_1|$, $|b_2|$, and the lowest energy exciton components are still located at $-(|b_1| + |b_2|)$. While the aggregates considered here likely contain $\sim$ one order of magnitude fewer pigments than the rodlike elements in chlorosomes (Staehelin et al., 1978), the predictable effects of the aggregate length r on the spectrum make the consideration of larger r unnecessary here. Increasing r does not influence the bandhead positions, but it quantitatively decreases the energy spacings between satellite bands as in a J-aggregate of the same length r and coupling a (cf. Eq. 2 and Fig. 3). In all of the calculations that follow, the pigment orientations in cases (a) through (c) yield *identical* spectra; the distinctions among these cases are therefore dropped from our discussion.

Since there is only one symmetry-allowed bandhead, the strongest transition always occurs to the lowest allowed exciton component when $a < 0$. This conflicts with experiment (Fetisova and Mauring 1992). The lowest allowed transition lies above the lowest-energy exciton component (Figure 4). For efficient energy transfers from the rodlike aggregates into the BChl *a*-protein baseplate antenna, the lowest-energy transition with substantial dipole strength in the aggregate must lie within $\sim kT$ of the transition to the lowest-energy exciton component. This does not occur for substantial b_1 and/or b_2. The observability of a 752 nm resonant zero-phonon hole at 1.8 K (Fetisova and Mauring 1992) requires that the lowest-energy exciton component in the model spectra carry significant oscillator strength. None of the spectra satisfy these combined requirements. Identical conclusions are reached for $2c = 12$, since the energy separations between the allowed bandhead and the lowest-energy transition are the same as those for $2c = 8$. An analogous situation occurs for $2c = 6$, where the bandheads appear at $b_1 + b_2$, $-(b + b_2)$, $\pm\sqrt{b_1^2 - b_1 b_2 + b_1^2}$; the only allowed bandhead in this case is the one at $|b_1| + |b_2|$.

Since no tubular model with $\mathbf{D}_{ch}$ or higher symmetry simulates the experimental spectrum, we consider symmetry-breaking effects. Figures 5 and 6 show exciton stick spectra computed by introducing *random* disorder into the Hamiltonian matrix elements. In Figure 5, each of the stick spectra shown in Figure 4 was modified by augmenting the *off-diagonal* element b_1 each time it appears in the Hamiltonian with a random number between $-0.4b_1$ and $+0.4b_1$, and similarly for b_2. In Figure 6, random *diagonal* disorder was simulated by assigning each of the elements H_{ii} (pre-

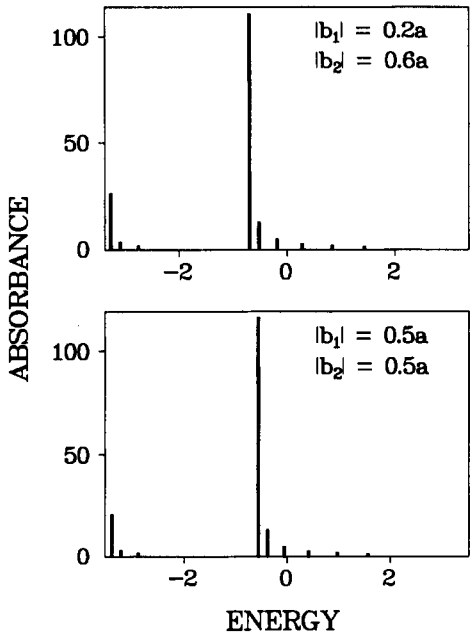

Figure 7. Schematic absorption spectra for the same tubular aggregates as in Fig. 4, except that the BChl *c* diagonal energies H_{ii} alternate between $-|a|$ and $+|a|$ from column to column (see text).

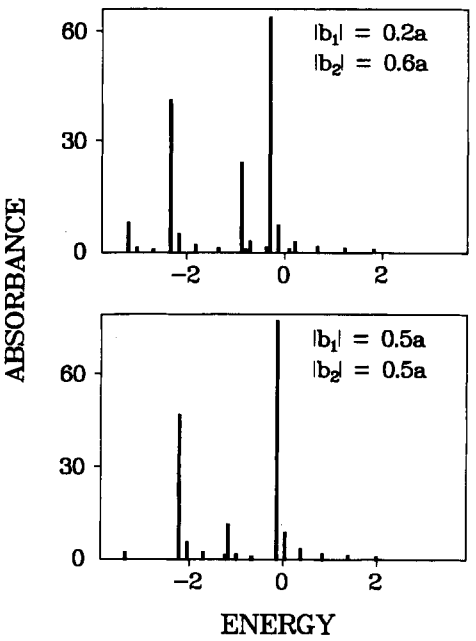

Figure 8. Schematic absorption spectra for tubular aggregates with $2c$=8 and r=20. Diagonal energies H_{ii} are $+|a|$ for pigments in columns 1 through c, and $-|a|$ for pigments in columns $(c+1)$ through $2c$.

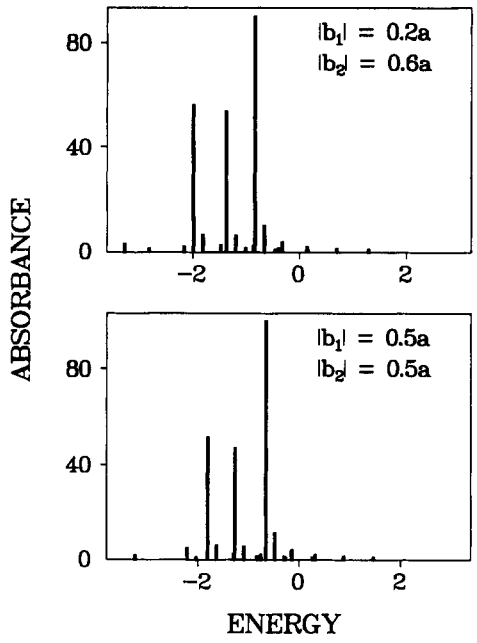

Figure 9. Schematic absorption spectra for tubular aggregates with $2c$=12 and r=20. Diagonal energies H_{ii} are $+0.25|a|$ in columns 1,2; $+0.5|a|$ in columns 3,4 $+0.25|a|$ in columns 5,6; $-0.5|a|$ in columns 7,8; $-|a|$ in columns 9,10; and $-0.5|a|$ in columns 11,12.

viously set equal to zero) a random number between $-a$ and a. While the randomness in both cases produces a partial breakdown in the selection rule that restricts allowed bandheads to the one located near $2a + |b_1| + |b_2|$, the maximum in the intensity distribution is essentially unshifted. In the presence of diagonal energy disorder (Figure 6), the spectra now resemble the experimental spectrum, in that the lowest-energy exciton component gains intensity and lies appreciably below the most intense transition. In order for the lowest exciton component to gain significant intensity in Figure 6, the width of the random distribution in diagonal energies must be at least comparable to the energy separation between the symmetry-allowed bandhead and the lowest-energy bandhead. In a calculation similar to that in Figure 6, but with diagonal energies ranging from $-0.2a$ to $+0.2a$ instead of from $+a$ to $-a$, the lowest-energy component exhibited only 0.005% of the intensity of the most intense component. For comparison, the ratio of absorption coefficients at the zero-phonon hole and at the band maximum for the BChl *c* antenna in whole cells of *Cf. aurantiacus* is ~ 0.1 (Fetisova and Mauring 1992).

We next consider *nonrandom* symmetry-breaking. In Figure 7, we show exciton stick spectra analogous to those in Figure 4, except that the diagonal energies

H_{ii} (set equal to zero in Figure 4) alternate from column to column: $H_{ii} = -a$ in columns 1, 3, ..., $(2c-1)$; and $H_{ii} = +a$ in columns 2, 4, ..., $2c$. This produces two allowed bandheads. For $2c = 8$ or 12, their positions are $\pm\sqrt{a^2 + (|b_1| + |b_2|)^2}$ relative to the unsplit bandhead. The less intense bandhead coincides with the lowest exciton component. Weaker alternations in H_{ii} produce less pronounced secondary bandheads. For example, a calculation for $b_1 = 0.2a$ and $b_2 = 0.6a$, with H_{ii} alternating between $-0.2a$ and $+0.2a$, yields a secondary bandhead with only ~1.5% of the intensity of the primary bandhead (not shown). This contrasts with the ~23% ratio obtained for the same b_1 and b_2 when H_{ii} alternates between $-a$ and $+a$ (Figure 7).

Figure 8 shows exciton stick spectra similar to those in Figure 4, except that the diagonal energies were set to $+|a|$ for columns 1 through c, and $-|a|$ for columns $(c + 1)$ through $2c$ (= 8 in Figure 8). (Environments experienced by the top and bottom cylindrical surfaces of rodlike elements can produce asymmetry of this type; the bottom surfaces of rods adjacent to the baseplate contact the baseplate, while the top surfaces contact other rodlike elements.) This situation produces at least three allowed bandheads. The most intense bandhead typically lies to the blue of several secondary bandheads. For the choices of b_1 and b_2 in Fig. 8, the lowest exciton component is forbidden. Very similar spectra are obtained for $2c = 12$.

Further symmetry-breaking is illustrated in Figure 9 for aggregates with $2c = 12$ and $r = 20$. Here the diagonal matrix elements are $+0.25|a|$ for the pigments in columns 1–2, $+0.5|a|$ in columns 3–4, $+0.25|a|$ in columns 5–6, $-0.5|a|$ in columns 7–8, $-|a|$ in columns 9–10, and $-0.5|a|$ in columns 11–12. (This is a variation on the symmetry-breaking in Figure 8, with a more gradual transition from positive to negative diagonal energies.) In some cases (depending on b_1 and b_2), the reduced symmetry increases the number of major bandheads; in others, the principal effect is intensity redistribution. In the models of Figs. 8–9, the lowest (forbidden) exciton component lies $0.025a$ to $0.050a$ below the lowest allowed bandhead. For $a \sim 700$ cm^{-1} (following Section), this corresponds to an energy separation of ~15–30 cm^{-1}. The existence of this lowest level would have little effect on the energy transfer function at physiological temperatures, but it would begin to influence the kinetics at temperatures in the low tens of K.

We comment briefly on the effects of including non-nearest neighbor interactions between pigments on adjacent columns. The only cross-couplings considered above are the matrix elements $H_{i,i\pm r}$ connecting pigments on the same disk (Figure 1). From Equation (1), the dipole-dipole coupling $H_{i,r+i\pm n}$ of pigment i to pigment $(r + i \pm n)$, which is located on the adjacent column, but displaced by n disks along that column, is

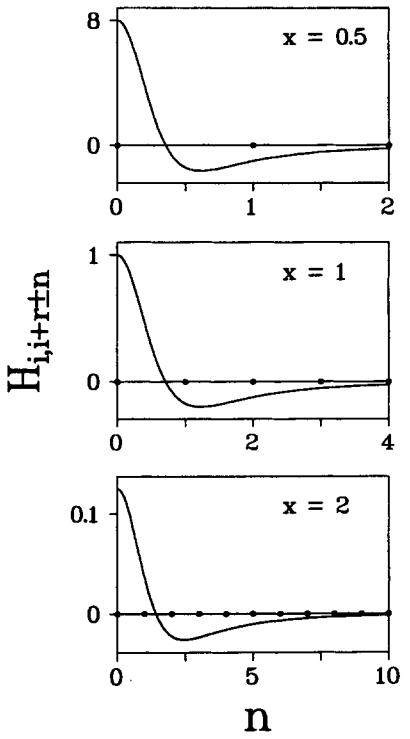

Figure 10. Cross-couplings $H_{i,i+r\pm n}$ between pigments on adjacent columns and displaced by n disks, plotted versus n for $d_a = 1$ and $\mu_i \cdot \mu_j = 1$. Bullets along the horizontal axis mark integral n, and emphasize that many cross-coupling terms need to be included when $x = d_b/d_a > 1$ (see text).

$$H_{i,i+r\pm n} = \frac{\mu_i \cdot \mu_j \left(1 - 3\frac{n^2}{n^2+x^2}\right)}{d_a^3 (n^2 + x^2)^{3/2}} \qquad (5)$$

Here, x is the ratio of spacings d_b/d_a between nearest-neighbor pigments on adjacent columns and on adjacent disks, respectively. This coupling is plotted versus n for $x = 0.5$, 1, and 2 in Figure 10. By the nature of the dipole-dipole orientational factor, this coupling switches sign as n increases from 0. It is clear from Figure 10 that when the column spacing is comparable to or shorter than the disk spacing ($x < 1$), $H_{i,r+i\pm}$ n falls off rapidly with n. In this limit, including non-nearest neighbor interactions alters the numerical levels and intensities, but does not affect the gross spectral features. When x becomes appreciably larger than 1 (i.e. when the column spacing is considerably larger than

the disk spacing), many non-nearest neighbor interactions gain importance, and many of these interactions for larger n exhibit sign opposite to that for $n = 0$. In this limit of wide column spacings, the inclusion of non-nearest neighbor interactions can thus change the physical spectrum significantly.

The BChl c spectrum in *Cf. aurantiacus*

In the absence of diagonal and/or off-diagonal energy disorder, the absorption spectra derived from our most symmetric ($\mathbf{D}_{2c,h}$ or $\mathbf{D}_{ch}$) tubular exciton models with $2c$ pigments per disk (Figure 4) clearly fail to explain the gross features of the BChl c Q_y antenna spectrum (Fetisova and Mauring 1992). Introducing sufficient random diagonal or off-diagonal disorder (but otherwise retaining at least $\mathbf{D}_{ch}$ symmetry) yields spectra which superficially resemble the empirical spectrum, in that transitions to the lowest-energy exciton component lie significantly to the red of the most intense exciton component (Figures 5–6). However, the extent of energy disorder required to produce observable intensities in the lowest-energy component (e.g. Figure 6) would be comparable to the $\sim$170 cm^{-1} separation between the 752 nm zero-phonon hole (ZPH) and the 742 nm band maximum. This would produce a commensurate spread in the ZPH location (i.e. in the sense that different random number sets yield different positions for the lowest-energy component), and this appears to be contradicted by the observation that the ZPH inhomogenous broadening is minor ($\leq$ 90 cm^{-1} according to Fetisova and Mauring (1992).

More realistic spectra are generated when the symmetry is reduced. For appropriate combinations of b_1 and b_2, alternation of the diagonal energies between $+|a|$ and $-|a|$ from column to column (Figure 7) produces a weak but observable transition to the lowest-energy bandhead, lying considerably to the blue of the strongest bandhead. The separation between these two components would need to be $\sim$170 cm^{-1} to model the experimental spectrum. The $\sim$90 cm^{-1} spectral width of the lowest-energy exciton component stems from a combination of inhomogeneous and lifetime broadening. The higher-energy components are likely to be somewhat broader, due to relaxation between BChl c exciton components.The expected lifetime broadening corresponding to a 100 fs relaxation process is $\sim$100 cm^{-1}fwhm. Photobleaching and stimulated emission decay components have been found with $\sim$70–100 fs lifetime in the BChl c pump-probe spectroscopy of intact chlorosomes from *Cf. aurantiacus* (Savikhin et al. 1994). Empirical 10–20 fs processes appear in pump-probe profiles for certain wavelength combinations in chlorosomes from *Cf. aurantiacus* and *Chlorobium tepidum* (Savikhin et al. 1995b). However, these likely arise from optical coherences at early times where the pump and probe pulses overlap, rather than from true one-exciton state evolution (Chachisvilis et al. 1995). Hence, we set an upper limit of $\sim$150 cm^{-1} for the total fwhm in the higher-energy exciton components. The featureless BChl c Q_y spectrum in chlorosomes cannot be simulated using only two bandheads separated by $\sim$170 cm^{-1}, with widths bounded from above by 90 and 150 cm^{-1}. Hence, the exciton stick spectra in Figure 7 appear to be far too sparse to rationalize the experimental spectrum. Further symmetry-breaking (by assigning the diagonal energies $+|a|$ and $-|a|$ to pigments in columns 1 through c and (c + 1) through $2c$, respectively) produces more congested spectra (Figure 8), but the bandhead distributions between the lowest-energy and the most intense components are still marginally dense (average spacing 90–100 cm^{-1}, for three bandheads distributed over $\sim$a 170 cm^{-1} span) for simulating the observed featureless spectrum. The least symmetric case considered (Figure 9) does appear to yield suitable bandhead spacings.

Thus, realistic BChl c spectra may readily be simulated using the models in Figure 9. However, the required extent of symmetry-breaking in the diagonal energies is quite large, on the order of $|a|$ itself. For example, if all of the diagonal energies H_{ii} for $b_1 = b_2 = 0.5a$ in Figure 9 were reduced by a factor of 2, the ratio of intensities for the lowest and the most intense exciton components would decrease from $\sim$0.1 to $\sim$0.01. In this case, the spectrum would more closely resemble the one where all of the $H_{ii} = 0$ (cf. bottom of Figure 4). Whether environmental differences between opposite rod surfaces can produce such large variations in diagonal energies is open to question. In order for the BChl c band maximum to be shifted from 670 nm (for BChl c monomers in solution) to 740 nm (for BChl c aggregates), a would need to be on the order of 700 cm^{-1}. The diagonal energies for the spectra simulated in Figure 9 would then range over 1050 cm^{-1} (i.e. from $+|a|/2$ = 350 cm^{-1} to $-|a|$ = –700 cm^{-1}). Lu and Pearlstein (1993) showed that the absorption spectrum of FMO trimers from the green bacterium *Prosthecochloris aestuarii* is consistent with BChl a diagonal energies dispersed over $\sim$600 cm^{-1} in the protein environment. Earlier calculations by Gudowska-Novak et al. (1991) suggested that the BChl a conformational

differences among the 7 non-equivalent pigments in FMO trimers (Tronrud et al. 1986) would of themselves produce diagonal disorder on the order of 500 cm^{-1}. As an alternative to the models in Figure 9, we considered an aggregate with $2c = 12$ and $r = 20$, in which the diagonal energies H_{ii} alternated between $+|a|$ and $-|a|$ from column to column, but in which the couplings $H_{i,i+r}$ varied in a geometric series from $|a|/2$ to $|a|/4$ between opposite faces of the rod. In particular, the (repulsive) couplings were $|a|/2$ between columns 1 and 2; $|a|/2^{7/6}$ between columns 2, 3 and 1, 12; $|a|/2^{4/3}$ between columns 3, 4 and 11, 12; $|a|/2^{3/2}$ between columns 4, 5 and 10, 11; $|a|/2^{5/3}$ between columns 5, 6 and 9, 10; $|a|\,2^{11/6}$ between columns 6, 7 and 8, 9; and $|a|/4$ between columns 7, 8 (which are on the opposite side of the rod from columns 1, 2). In the dipole-dipole approximation, these couplings would result from systematic variation in column spacings around the rod perimeter, in such a way that adjacent column spacings differ by a factor of $2^{1/2}$. The resulting spectrum (not shown) strongly resembles the simulations in Figure 7; this type of symmetry-breaking in the couplings thus appears to have little effect.

With their rudimentary transition moment geometries (Figure 2), our models do not explain why BChl *c* antennae in chlorosomes exhibit wavelength-dependent linear and circular dichroism (van Amerongen et al. 1988; Griebenow et al. 1991; Matsuura et al. 1993; Chiefari et al. 1995). These features may be addressed by introducing some chirality into the transition moment orientations, as suggested by Lin et al. (1991). In aggregate models with noncollinear pigments, different exciton components will generally exhibit contrasting linear dichroism. Finally, since our model only considers vibrationless electronic transitions with lifetime and inhomogeneous broadening, it will underestimate the absorption coefficient on the blue side of the BChl *c* Q_y spectrum, where vibronic features become important.

Summary

Our primary goal was to find the simplest homogeneous exciton models that could rationalize the electronic spectroscopy of BChl *c* antennae in chlorosomes from *Cf. aurantiacus*. For the class of models in Figures 1–2, the required properties are:

(i) The transition moments must be oriented at <54.7° from the aggregate axis, in order for the aggregate spectrum to concentrate dipole strength to the red of the monomeric BChl *c* Q_y transition at ~670 nm. In this respect, the BChl *c* oligomer spectrum is analogous to a J-aggregate, rather than H-aggregate spectrum.

(ii) Significant symmetry-breaking is required in order to yield a multiplet of dipole-allowed bandheads with a realistic intensity distribution (Figures 7–9). Tubular exciton models with $\mathbf{D}_{2c,h}$ and $\mathbf{D}_{ch}$ symmetry are inconsistent with the observed spectrum.

(iii) The energy spacings between major bandheads must be appreciably less than ~100 cm^{-1} (e.g. as in Figure 9), in order to reproduce the broad, featureless nonresonant hole observed by Fetisova and Mauring (1992).

(iv) The simulated absorption spectra are relatively insensitive to the aggregate length r when r is large, since in this limit the satellite bands merge with the bandhead (Figure 3).

Aside from introducing transition moment chirality, further refinements of this model may require consideration of spectral heterogeneity. In particular, the diagonal energy distribution in H_{ii} for pigments around the periphery of a cylindrical rodlike element may may depend on whether the rod is adjacent or nonadjacent to the baseplate. Thus, while a particular rod may exhibit a homogeneously broadened spectrum with ~200 cm^{-1} fwhm (cf. Fetisova and Mauring 1992), other rods may exhibit shifted (but similarly broad) spectra.

Acknowledgements

The Ames Laboratory is operated for the US Department of Energy by Iowa State University under Contract No. W-7405-Eng-82. This work was supported by the Division of Chemical Sciences, Office of Basic Energy Sciences. We are indebted to Herbert van Amerongen for his assistance in earlier stages of this work.

Note

1. This is correct for a J-aggregate with parallel transition moments (as in Figure 2). For a J-aggregate in which neighbouring moments are antiparallel, this is correct when $a>0$. In either case, the moments must form an angle <54.7° with respect to the aggregate axis.

References

Alden RG, Lin SH and Blankenship RE (1992) Theory of spectroscopy and energy transfer of oligomeric pigments in chlorosome antennas of green photosynthetic bacteria. J Lumin 51: 51–66

Blankenship RE, Brune DC and Wittmershaus BP (1988) Chlorosome antennas in green photosynthetic bacteria. In: Stevens SE Jr and Bryant DA (eds) Light Energy Transduction in Photosynthesis: Higher Plant and Bacterial Models, pp 32–64. American Society of Plant Physiologists, Rockville, MD

Blankenship RE, Olson JM and Miller M (1995) Antenna complexes from green photosynthetic bacteria. In: Blankenship RE, Madigan MT and Bauer CE (eds) Anoxygenic Photosynthetic Bacteria, pp 399–431. Kluwer Academic Publishers, Dordrecht

Brune DC, Nozawa T and Blankenship RE (1987) Antenna organization in green photosynthetic bacteria. 1. Oligomeric bacteriochlorophyll *c* as a model for the 740 nm absorbing bacteriochlorophyll *c* in *Chloroflexus aurantiacus* chlorosomes. Biochemistry 26: 8644–8652

Brune DC, King GH and Blankenship RE (1988) Interactions between Bacteriochlorophyll *c* molecules in oligomers and in chlorosomes of green photosynthetic bacteria. In: Scheer H and Schneider S. (eds) Photosynthetic Light-Harvesting Systems, pp 141–151. Walter de Gruyter, Berlin

Bystrova MI, Mal'gosheva IN and Krasnovskii AA (1979) Study of molecular mechanism of self-assembly of aggregated forms of BChl *c*. Mol Biol (English Trans) 13: 582–594

Chachisvilis M, Fidder H and Sundström V (1995) Electronic coherence in pseudo two-color pump-probe spectroscopy. Chem Phys Lett 234: 141–150

Chiefari J, Griebenow K, Griebenow N, Balaban TS, Holzwarth AR and Schaffner K (1995) Models for the pigment organization in the chlorosomes of photosynthetic bacteria: Diastereoselective control of *in-vitro* bacteriochlorophyll c_S aggregation. J Phys Chem 99: 1357–1365

Fetisova Z and Mauring K (1992) Experimental evidence of oligomeric organization of antenna bacteriochlorophyll *c* in green bacterium *Chloroflexus aurantiacus* by spectral hole burning. FEBS Lett 307: 371–374

Griebenow K, Holzwarth AR, van Mourik F and van Grondelle R (1991) Pigment organization and energy transfer in green bacteria. 2. Circular and linear dichroism spectra of protein-containing and protein-free chlorosomes isolated from *Chloroflexus aurantiacus* strain Ok-70-fl$^+$. Biochim Biophys Acta 1058: 194–202

Gudowska-Nowak E, Newton MD and Fajer J (1991) Conformational and environmental effects on bacteriochlorophyll optical spectra: correlation of calculated spectra with structural results. J Phys Chem 94: 5795–5801

Holzwarth AR and Schaffner K (1994) On the structure of bacteriochlorophyll molecular aggregates in the chlorosomes of green bacteria. A molecular modeling study. Photosynth Res 41: 225–233

Lin S, van Amerongen H and Struve WS (1991) Ultrafast pump-probe spectroscopy of bacteriochlorophyll *c* antennae in bacteriochlorophyll *a* - containing chlorosomes from the green bacterium *Chloroflexus aurantiacus*. Biochim Biophys Acta 1060: 13–24

Lu XY and Pearlstein RM (1993) Simulations of *Prosthecochloris* bacteriochlorophyll *a* protein optical spectra improved by parametric computer search. Photochem Photobiol 57: 86–91

Lutz M and van Brakel G (1988) Ground-state molecular interactions of bacteriochlorophyll *c* in chlorosomes of green bacteria and in model systems: A resonance Raman study. In: Olson JM, Ormerod JG, Amesz J, Stackebrandt E and Trüper HG (eds) Green Photosynthetic Bacteria, pp 23–34. Plenum Press, New York

Matsuura K, Hirota M, Shimada K and Mimuro M (1993) Spectral forms and orientation of bacteriochlorophylls *c* and *a* in chlorosomes of the green photosynthetic bacterium *Chloroflexus aurantiacus*. Photochem Photobiol 57: 92–97

Mimuro M, Nozawa T, Tamai N, Shimada K, Yamazaki I, Lin S, Knox RS, Wittmershaus BP, Brune DC and Blankenship RE (1989) Excitation energy flow in chlorosome antennas of green photosynthetic bacteria. J Phys Chem 93: 7503–7509

Nozawa T, Ohtomo K, Suzuki M, Morishita Y and Madigan MT (1993) Structures and organization of bacteriochlorophyll *c*'s in chlorosomes from a new thermophilic bacterium *Chlorobium tepidum*. Bull Chem Soc Japan 66: 231–237

Nozawa T, Ohtomo K, Suzuki M, Nakagawa H, Shikama Y, Konami H and Wang Z-Y (1994) Structures of chlorosomes and aggregated BChl *c* in *Chlorobium tepidum* from solid state high resolution CP/MAS ^{13}C NMR. Photosynth Res 41: 211–223

Savikhin S, Zhu Y, Lin S, Blankenship RE and Struve WS (1994) Femtosecond spectroscopy of chlorosome antennas from the green photosynthetic bacterium *Chloroflexus aurantiacus*. J Phys Chem 98: 10322–10334

Savikhin S, van Noort PI, Zhu Y, Lin S, Blankenship RE and Struve WS (1995a) Ultrafast energy transfer in light-harvesting chlorosomes from the green photosynthetic bacterium *Chlorobium tepidum*. Chem Phys 194: 245–258

Savikin S, van Noort PI, Blankenship RE and Struve WS (1995b) Femtosecond probe of structural analogies between chlorosomes and bacteriochlorophyll *c* aggregates. Biophys J 69: 1100–1104

Somsen O (1995) Excitonic interaction in photosynthesis: migration and spectroscopy PhD Thesis. Free University, Amsterdam

Smith LA Kehres LA and Fajer J (1983) Aggregation of the bacteriochlorophylls *c*, *d*, and *e*. Models for the antenna chlorophylls of green and brown phoosynthetic bacteria. J Am Chem Soc 105: 1387–1389

Staehelin LA, Golecki JR, Fuller RC and Drews G (1978) Visualization of the supramolecular architecture of chlorosomes (*Chlorobium* type vesicles) in freeze-fractured cells of *Chloroflexus aurantiacus*. Arch Microbiol 119: 269–277

Struve WS (1989) Fundamentals of Molecular Spectroscopy, pp 267–275. Wiley-Interscience, New York

Tronrud DE, Schmid MR and Matthews BW (1986) Structure and X-ray amino acid sequence of a bacteriochlorophyll *a* protein from *Prosthecochloris aestuarii* refined at 1.9 Å resolution. J Mol Biol 188: 443–454

Van Amerongen H, Vasmel H and van Grondelle R (1988) Linear dichroism of chlorosomes from *Chloroflexus aurantiacus* in compressed gels and electric fields. Biophys J 54: 65–76

Van Noort PI, Francke C, Schoumans N, Otte SCM, Aartsma T and Amesz J (1994) Chlorosomes of green bacteria: Pigment composition and energy transfer. Photosynth Res 41: 193–203